

# On variability and interdependence of local porosity and local tortuosity in porous materials: a case study for sack paper

Matthias Neumann · Eduardo Machado Charry · Karin Zojer · Volker Schmidt

Received: date / Accepted: date

**Abstract** The variability and interdependence of local porosity and local mean geodesic tortuosity, which is a measure for the sinuosity of shortest transportation paths, is investigated at the example of the microstructure in sack paper. By means of statistical image analysis, these two morphological characteristics are computed for several cutouts of 3D image data obtained by X-ray microcomputed tomography. Considering cutouts of different sizes allows us to study the influence of the sample size on the local variability of the considered characteristics. Moreover, the interdependence between local porosity and local mean geodesic tortuosity is quantified by modeling their joint distribution parametrically using Archimedean copulas. It turns out that the family of Gumbel copulas is an appropriate model type, which is formally validated by a goodness of fit test. Besides mean geodesic tortuosity, we consider further related morphological characteristics, describing the sinuosity of those shortest transportation paths, whose minimum diameter exceeds a predefined threshold. Moreover, we show that the copula approach investigated in this paper can also be used to quantify the negative correlation between local porosity and these modified versions of local mean geodesic tortuosity. Our results elucidate the impact of local porosity on various kinds of morphological characteristics, which are not experimentally accessible and which are important for local air permeance – a key property of sack paper.

**Keywords** Sack paper ·  $\mu$ -CT · porosity · tortuosity · statistical microstructure analysis · parametric copula model

**Mathematics Subject Classification (2010)** 62H11 · 62P30

---

M. Neumann · V. Schmidt  
Institute of Stochastics, Ulm University, Helmholtzstraße 18, 89069 Ulm, Germany, Tel.: +49-731-5023617 E-mail: matthias.neumann@uni-ulm.de

E. Machado Charry · K. Zojer  
Institute of Solid State Physics and NAWI Graz, Graz University of Technology, Petersgasse 16/III, 8010 Graz, Austria

E. Machado Charry · K. Zojer  
Christian Doppler Laboratory for Mass Transport through Paper, Graz University of Technology, Petersgasse 16/III, 8010 Graz, Austria

## 1 Introduction

One of the major questions when studying porous materials is the relationship between the morphology of the pore space and the corresponding macroscopic properties [29]. To investigate this kind of problems, the combination of tomographic 3D imaging and subsequent image analysis is a powerful tool, which allows for the computation of morphological characteristics that are experimentally not accessible [6, 22, 26]. Typically, these morphological characteristics are globally aggregated characteristics. Such global characteristics are, in principle, defined for unboundedly large microstructures that feature a certain spatial homogeneity [6].

Mathematically speaking, these microstructures can be considered as realizations of stationary random sets. When estimating such characteristics from image data, local fluctuations of the microstructure play an important role. On the one hand, local fluctuations determine the minimum size of the investigated microstructure or a subset thereof such that the estimates of morphological characteristics are representative [1, 7, 14, 24]. On the other hand, it is highly desirable to quantify the local variability of morphological characteristics itself. A variability in morphological characteristics of a porous material inherently leads to a variability in its macroscopic properties. This is illustrated with the dependence of effective transport properties on a locally varying porosity [12]. For example, the relationship between univariate distributions of local porosity and local conductivity of sandstone is investigated in [27]. For a comprehensive discussion of fluctuations of local volume fractions, we refer to Chapter 11 in [29] and the references therein.

In the present article, we investigate the variability of local porosity and local mean geodesic tortuosity [20] for a paper-based material. The mean geodesic tortuosity is a descriptor for the sinuosity of shortest transportation paths through the pore space. In going beyond our previous exploratory study [21], where we only considered mean geodesic tortuosity, we account for the length of shortest transportation paths with several local descriptors. Our selection of descriptors discriminate paths not only in terms of their sinuosity, but also with respect to possibly encountered ‘bottlenecks’. Each of these descriptors is related to a predefined threshold. For a given threshold, the corresponding descriptor measures the lengths of those shortest transportation paths, whose minimum diameter exceeds the threshold. In other words, only those paths are considered, which can be traversed by balls with a diameter corresponding to the predefined threshold.

We expect the lengths of shortest transportation paths to strongly relate to the air permeance through paper [2], in particular for the sack paper considered in the present article. Sack paper is used for the packing of powdered goods. Thus, the air permeance is – besides tensile energy absorption – its most important macroscopic property, since it allows an efficient de-aeration of bags during filling [11]. Hence, the descriptors derived from the mean geodesic tortuosity are, besides porosity, important morphological characteristics of sack paper. The main objective of the present paper is to quantitatively assess the variability and interdependence of these morphology-related descriptors, in particular their correlation. For this purpose, we proceed as follows. First, we determine each individual descriptor from image data obtained by X-ray microcomputed tomography ( $\mu$ -CT), see [16]. Second, utilizing copulas [4, 19], we then construct a parametric The selected model type for the copula, *i.e.*, the family of Gumbel copulas, has the major advantage, that it is appropriate to model the joint distribution of porosity and the path-

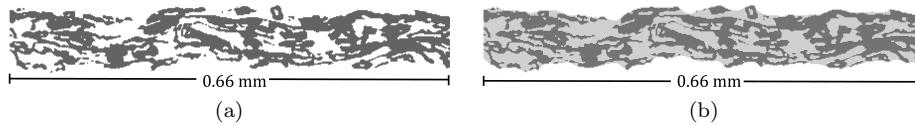


**Fig. 1** Cutout of a 2D slice of the binarized image data corresponding to a vertical cross-section through the paper sheet. Shown is the cutout before (a) and after determination of the inner pore space (b). The cellulose material (fibers) and the inner pore space are represented in dark and bright grey, respectively.

length related descriptors for differently chosen values of the diameter threshold of the latter. Moreover, the model fits well for different sizes of the considered local environment and it leads to an improvement of the fit compared to the Frank copula used in [21]. Having fitted the parametric model for the joint distributions, trends with respect to variability and interdependence of the considered local descriptors can be quantified by the parameter of the Gumbel copula. Moreover, we directly obtain the conditional distribution of the path-length related descriptors for a given local porosity. Thereby, we particularly focus on the influence of the threshold parameter appearing in the definition of the path-length related descriptors, which leads to new insights going beyond the results presented in [21]. Summarizing, the presented parametric modeling approach has the following advantages compared to a non-parametric approach. It enables us to show that even if the distributions of local characteristics computed from cutouts with varying sizes are different, they still have a similar structure since one and the same model type leads to an appropriate fit. Moreover, the complexity of data is strongly reduced to the low-dimensional parameter space and the distributions under consideration can be analytically expressed, which leads, in turn, to analytical expressions for the conditional distribution of local path-length related descriptors for given local porosity. Thereby the variability and interdependence of local porosity and local path-length related descriptors which are assumed to be essential for air permeance in sack paper are quantified by means of the model parameters and their interpretation is reduced to the interpretation of the parameters of the distribution.

## 2 Materials and Imaging

Our analysis is based on sack paper made of unbleached pulp with a specific basis weight of  $70 \text{ g/m}^2$ . The latter value, which corresponds to the supplier specifications, is confirmed by a test in accordance to the standard DIN EN ISO 536 (Paper and board: Determination of grammage). This type of sack paper is employed to produce cement bags and thus, combines a high porosity with a superior mechanical strength.

The 3D microstructure of the considered material is deduced from  $\mu$ -CT images. The imaging is performed using an Xradia 500 Versa 3D X-ray microscope (Zeiss, Germany). The isotropic voxels have an edge length of  $1.5 \text{ }\mu\text{m}$  and the final image has a size of  $2.001 \text{ mm} \times 2.802 \text{ mm} \times \text{thickness}$  after binarization. For detailed information regarding the experimental setup, the preprocessing, and the binarization of image data, we refer to [16].

As illustrated in Figure 1a, the microstructure obtained after binarization consists of fibers (dark), mainly formed of cellulose, and pores (white). A key step in determining the porosity of paper material from 3D image data is the definition of the top and bottom surfaces of the paper sheet. This is particularly important for paper types exhibiting a large surface roughness and thus a large variability of local thickness (cf. Figure 1a). The so-called rolling ball approach [5] is the most reasonable method to define each surface [16], since it accurately represents the inherent roughness of the surface. A ball with a given radius (here 15  $\mu\text{m}$ ) is following ('rolling along') the surface formed of the cellulose material. All voxels that cannot be reached by the ball are then assigned to the inner pore space, *i.e.*, to the set of voids that form the pores within the paper and in which transport paths are established. Figure 1b illustrates the distinction between this inner pore space (light gray) from the surrounding void space (white) in the cross-section shown in Figure 1a after applying the rolling ball algorithm.

### 3 Local heterogeneity of the 3D microstructure

In order to quantify the local heterogeneity of the 3D microstructure, we consider a set of non-overlapping cutouts taken from the complete image data representing the microstructure of sack paper. Let the  $z$ -direction indicate the transversal direction connecting top and bottom paper surface. Then, a sensible three-dimensional cutout is square-shaped in the  $xy$ -plane and contains the complete microstructure in  $z$ -direction. As indicated in Figure 2 the centers of the squares are arranged in a square grid with a side length of 150  $\mu\text{m}$  that is imposed on the  $xy$ -plane. Given that the cutouts must not overlap, our setting leads to a total number of 204 cutouts. The side length of the squares, defining the cutout size in the  $xy$ -plane, is varied from 30  $\mu\text{m}$  to 60  $\mu\text{m}$ , 90  $\mu\text{m}$ , 120  $\mu\text{m}$ , and 150  $\mu\text{m}$ .

With the set of cutouts at hand, the quantification of the local heterogeneity encompasses three distinct methodological steps. First, we determine the porosity and the descriptors that measure the sinuosity of transportation paths through the pore space of these cutouts. The univariate distribution of the considered descriptors is modeled parametrically, where we capture the change in distribution of the descriptors with increasing cutout size. Secondly, we also model the joint bivariate distribution of these morphological characteristics parametrically for each cutout size. The fitted parametric model of the joint bivariate distribution quantifies the relationship between porosity and descriptors for the sinuosity of transportation paths and it allows us to compute the conditional distribution of local descriptors related to path lengths for a given value of local porosity. In the last step, we provide a validation of our copula model. A discussion of the results regarding the local variability and interdependence between the considered morphological characteristics is given separately in Section 4.

#### 3.1 Local porosity and local mean geodesic tortuosity

For each cutout, the local porosity is computed in the following way. At first, the top and bottom surfaces, *i.e.*, the boundaries of sack paper in  $z$ -direction, are determined as described in Section 2. Then, the local porosity of a cutout is defined

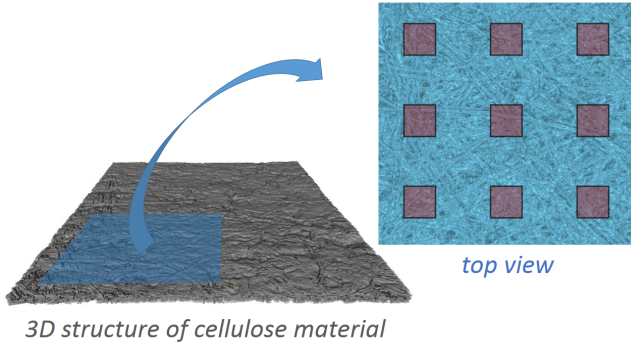


**Fig. 2** Square-shaped cutouts in  $xy$ -plane (red), arranged on a square grid, are considered to investigate the local heterogeneity of the 3D microstructure.

as the ratio of pore voxels to all voxels, which are contained in the cutout and which are located between the top and bottom surface. We assume stationarity of the microstructure of the considered sack paper with respect to translations in the  $xy$ -plane, which is a rather natural assumption. Thus the local porosities in the different cutouts are identically distributed, *i.e.*, the local porosities are considered as copies of one and the same random variable, denoted by  $P$ . Note that the distribution of  $P$  depends on the size of the cutout. If  $P$  refers to a specific cutout size, the size is explicitly given in the following.

Having computed the local porosity for all cutouts, we obtain a sequence of local porosities for each cutout size, see Figure 3a. The resulting histograms can be well modeled by the densities of beta-distributions [13]. The beta-distribution is a univariate probability distribution with probability density function  $f : \mathbb{R} \rightarrow [0, \infty)$  defined by

$$f(p) = \frac{\Gamma(a+b)}{\Gamma(a)\Gamma(b)} p^{a-1} (1-p)^{b-1} \mathbb{1}_{0 \leq p \leq 1}, \quad (1)$$

for each  $p \in \mathbb{R}$ , where  $a, b > 0$  are some parameters,  $\mathbb{1}$  denotes the indicator function, and  $\Gamma$  the gamma function. The parameters  $a$  and  $b$  are fitted via maximum likelihood estimation as described in [3]. The probability density functions of the fitted beta-distributions, that are shown in Figure 3b, indicate a good accordance with the local porosities from image data (Figure 3a).

Note that the distributions of local porosities in Figure 3a can also be well described by normal distributions. Normally distributed random variables take values smaller than 0 and larger than 1 with positive probability. In contrast, a random variable following the law of a beta-distribution only takes values between 0 and 1 with probability 1, as the support of the beta-distribution is the interval  $[0, 1]$ . Thus, the beta distribution is inherently more appropriate to model the distribution of local porosities.

Besides local porosity, we investigate the local behavior of mean geodesic tortuosity. Being a purely geometrical descriptor, mean geodesic tortuosity  $\tau$  (applied to sack paper) is the average of shortest path lengths from the bottom surface to the top surface divided by the local thickness of the sack [16]. To compute the mean geodesic tortuosity of a cutout, we average only over those paths, the starting points of which are located in the considered cutout. The paths themselves,

however, are allowed to leave the cutout. Otherwise we would introduce a bias into our computations as the boundary effects would have a stronger impact on local mean geodesic tortuosity of smaller cutouts. For a formal definition of mean geodesic tortuosity in the framework of random closed sets, we refer to [20]. To compute the shortest path lengths from 3D image data for given starting points, we use the Dijkstra algorithm [28] on the voxel grid. In addition to the mean geodesic tortuosity  $\tau$ , we consider modifications  $\tau^{(r)}$  of mean geodesic tortuosity, where only those paths are considered which permit the passage of a ball of radius  $r > 0$ . We investigate the case of mean geodesic tortuosity  $\tau = \tau^{(0)}$  ( $r = 0$ ) as well as the two modifications with  $r = 1.5 \mu\text{m}$  and  $r = 3 \mu\text{m}$ , *i.e.*,  $\tau^{(1.5)}$  and  $\tau^{(3.0)}$ . A step size of  $1.5 \mu\text{m}$  is used between the different values of  $r$ , since  $1.5 \mu\text{m}$  is the edge length of the cubic voxels, see Section 2. The largest value of  $r$  considered in the present paper is  $3.0 \mu\text{m}$ , since only a small amount of the pore space is accessible via an intrusion of spheres with a radius being larger than  $3.0 \mu\text{m}$ , see Figure 9 in [16].

Note that for each fixed  $r \geq 0$  and any given cutout,  $\tau^{(r)}$  is a random variable, where we assume – as for local porosity – that its distribution does not depend on which particular cutout is considered. If  $\tau^{(r)}$  refers to a specific cutout size, this is explicitly stated in the following.

The distribution of local mean geodesic tortuosities, visualized in Figure 3c, can be well modeled by a shifted generalized gamma-distribution [13] with probability density function  $g : \mathbb{R} \rightarrow [0, \infty)$  given by

$$g(t) = \frac{k(t-1)^{d-1}}{\alpha^d \Gamma\left(\frac{d}{k}\right)} e^{-\left(\frac{t-1}{\alpha}\right)^k} \mathbb{1}_{t \geq 1}, \quad (2)$$

for each  $t \in \mathbb{R}$ , where  $\alpha, d, k > 0$  are the parameters of the distribution. Note that the support of the generalized gamma-distribution considered in Equation (2) is the interval  $[1, \infty)$ . The parameters  $\alpha, d$ , and  $k$  are fitted by means of maximum likelihood estimation, where the maximization of the log-likelihood function is performed using the Nelder-Mead algorithm [18]. The probability density functions of the fitted shifted gamma distributions are shown in Figures 3d, 3f, 3h, respectively. One can observe that these probability density functions model appropriately the histograms computed from image data (see Figures 3c, 3e, 3g).

For the parametric distributions modeling the univariate distributions of porosity and the three path-length related descriptors, a formal validation is performed by means of the Kolmogorov-Smirnov test. In all cases, the test does not reject the null hypothesis that the considered data is a realization of the corresponding fitted parametric distribution at the level of 5 %. The  $p$ -values are listed in the appendix, where we also provide the numerical values of the fitted model parameters, *i.e.*, the obtained estimators for  $a, b, \alpha, d$ , and  $k$ .

### 3.2 Joint distribution of local porosity and local mean geodesic tortuosity

In this section, the interdependence of local porosity and local path length related descriptors is determined based on the data of the cutouts considered in the previous Section 3.1. In principle, the interdependence can be straight-forwardly investigated considering empirical bivariate distribution, that we can directly compute from tomographic image data. Here, we deliberately establish a parametric

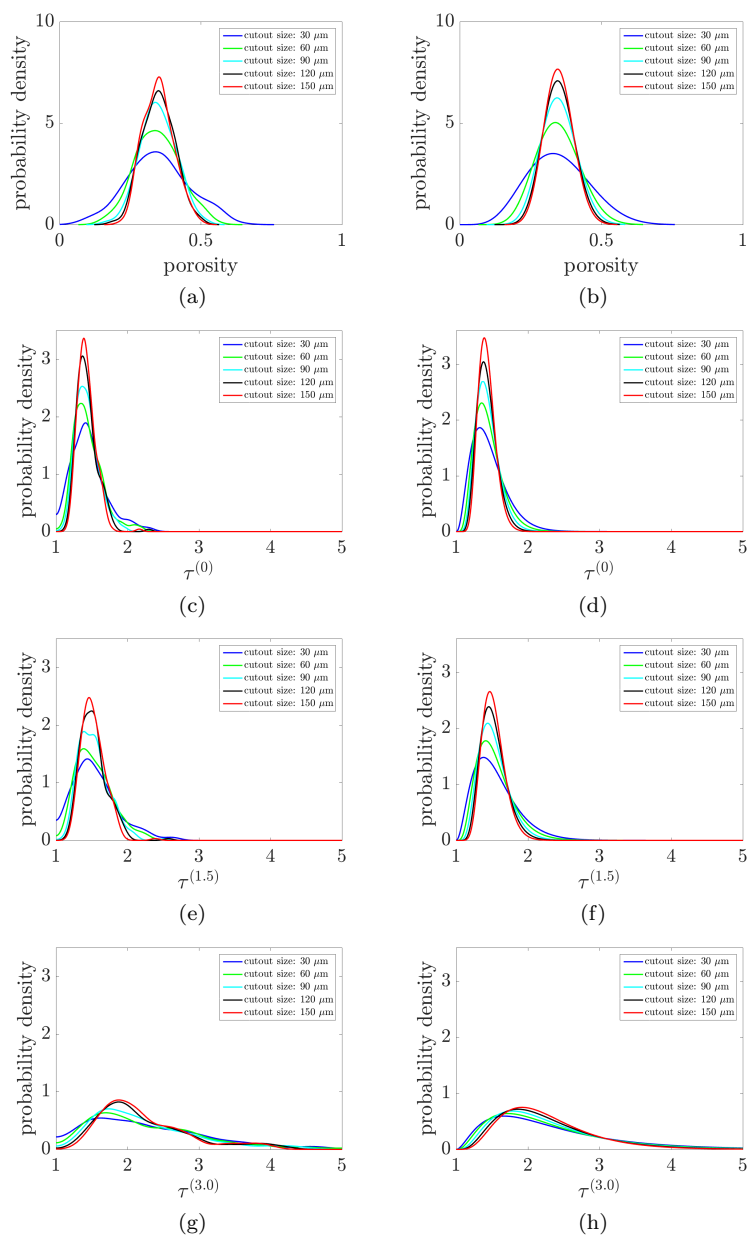


**Fig. 3** Comparison between the probability density distributions computed empirically from image data (left panels) and from the corresponding fitted beta and gamma distributions, respectively (right panels). Local porosity (a,b), and the descriptors derived from the mean geodesic tortuosities  $\tau^{(0)}$  (c,d),  $\tau^{(1.5)}$  (e,f), and  $\tau^{(3.0)}$  (g,h) are shown.

bivariate distribution prior evaluating the interdependence. For this purpose, we use so-called copulas, which are an appropriate tool to model bivariate distributions for given univariate marginal distributions. The use of copulas leads to several benefits. The main advantage is that the complexity of modeling the bivariate distribution is split up into modeling the univariate marginal distributions and modeling the copula, where the latter contains all the information about the interdependence between local porosity and the local path length related descriptors. This enables us to interpret the considered interdependence by interpreting the parameters of the copula. Note that the copula model used in the present paper has only one real-valued parameter. Moreover, the copula approach is quite flexible by allowing for arbitrary models for the univariate distribution and to combine them with an arbitrary parametric family of copulas.

A two-dimensional copula is the joint probability distribution function  $C : [0, 1]^2 \rightarrow [0, 1]$  of a random vector  $(U, V)$  taking values in  $[0, 1]^2$  with probability 1 where both marginals of  $(U, V)$  are uniformly distributed on the unit interval [25]. In particular, we have for all  $0 \leq u, v \leq 1$  that  $C(u, v) = \mathbb{P}(U \leq u, V \leq v)$ ,  $\mathbb{P}(U \leq u) = u$  and  $\mathbb{P}(V \leq v) = v$ . Sklar's theorem [19], a fundamental result of copula theory, states that for an arbitrary pair of random variables  $P$  and  $\tau^{(r)}$  with univariate distribution functions  $F : \mathbb{R} \rightarrow [0, 1]$ ,  $F(p) = \mathbb{P}(P \leq p)$  and  $G : \mathbb{R} \rightarrow [0, 1]$ ,  $G(t) = \mathbb{P}(\tau^{(r)} \leq t)$ , respectively, there exists a copula  $C$  which admits the representation

$$H(p, t) = C(F(p), G(t)) \quad (3)$$

of the joint distribution function  $H : \mathbb{R}^2 \rightarrow [0, 1]$  of  $P$  and  $\tau^{(r)}$ , for all  $p, t \in \mathbb{R}$ . Recall that in our case,  $P$  and  $\tau^{(r)}$  denote the random local porosity and the random modified local mean geodesic tortuosity for given  $r \geq 0$ , respectively, of a cutout of predefined size. If the random vector  $(P, \tau^{(r)})$  has the joint probability density function  $h : \mathbb{R}^2 \rightarrow [0, \infty)$ , we immediately obtain a formula for  $h$  from Equation (3), namely

$$h(p, t) = f(p)g(t) \left( \frac{\partial^2}{\partial p \partial t} C \right) (F(p), G(t)), \quad (4)$$

where  $f : \mathbb{R} \rightarrow [0, \infty)$  and  $g : \mathbb{R} \rightarrow [0, \infty)$  are the univariate probability density functions of  $P$  and  $\tau^{(r)}$ , respectively. Note that using Equation (4), one can easily derive the probability density function  $h_{\tau^{(r)}|P=p} : \mathbb{R}^2 \rightarrow [0, \infty)$  of the conditional distribution of  $\tau^{(r)}$  given that  $P = p$  for each  $p$  with  $f(p) > 0$  or vice versa. To be precise, from Equation (4) we obtain that

$$h_{\tau^{(r)}|P=p}(t) = \frac{h(p, t)}{f(p)} = g(t) \left( \frac{\partial^2}{\partial p \partial t} C \right) (F(p), G(t)) \quad (5)$$

for all  $p, t \in \mathbb{R}$  with  $f(p) > 0$ . This means that the copula approach allows us to compute the conditional probability density function of local mean geodesic tortuosity for a given local porosity – and vice versa, since the conditional distribution of  $P$  for given  $\tau^{(r)}$  is obtained analogous to Equation (5).

To model the data at hand, we select the family of Gumbel copulas as a model type. We compared the fits obtained with one-parametric families of so-called Archimedean copulas, see Chapter 4 in [19], *i.e.*, with the family of Gumbel and Clayton copulas to fits with copulas of the Frank type. This comparison revealed

**Table 1** Estimated values  $\hat{\lambda}$  of  $\lambda$  for different cutout sizes and tortuosities  $\tau^{(0)}$ ,  $\tau^{(1.5)}$  and  $\tau^{(3.0)}$ . The parameter  $\lambda$  quantifies the dependence between the local porosity and the respective local mean geodesic tortuosity for given cutout sizes.

side length of cutouts	30 $\mu\text{m}$	60 $\mu\text{m}$	90 $\mu\text{m}$	120 $\mu\text{m}$	150 $\mu\text{m}$
$\hat{\lambda}$ for $\tau^{(0)}$	1.41	1.46	1.59	1.68	1.73
$\hat{\lambda}$ for $\tau^{(1.5)}$	1.47	1.51	1.67	1.74	1.77
$\hat{\lambda}$ for $\tau^{(3.0)}$	1.24	1.30	1.50	1.67	1.74

that Gumbel copulas achieve a description that is superior to Frank copulas, even though Frank copula type were already shown to appropriately model the correlation between local porosity and local mean geodesic tortuosity in sack paper [21]. The choice of Gumbel copulas is formally validated in Section 3.3. Note that negative correlations cannot be directly modelled by means of the Gumbel copula, see Example 5.4 in [19]. Since a preliminary assessment of the data indicated a negative correlation between local porosity and local mean geodesic tortuosity [21], the Gumbel copula requires us to model the distribution of the random vector  $(P, \tau^{(r)})$  indirectly by modeling  $(P, -\tau^{(r)})$ . This joint distribution of  $P$  and  $-\tau^{(r)}$  uniquely defines the joint distribution of  $P$  and  $\tau^{(r)}$ .

The Gumbel copula  $C_\lambda$  with parameter  $\lambda \geq 1$  is defined by

$$C_\lambda(u, v) = \exp\left(-\left((-\log u)^\lambda + (-\log v)^\lambda\right)^{1/\lambda}\right) \quad (6)$$

for all  $0 \leq u, v \leq 1$ . If the parameter  $\lambda$  equals 1, then the Gumbel copula coincides with the product copula, which is equivalent to the independence of  $P$  and  $-\tau^{(r)}$ . The larger the value of  $\lambda$  is the stronger is the positive correlation between  $P$  and  $-\tau^{(r)}$  and, thus, the more negative correlation between  $P$  and  $\tau^{(r)}$ .

The parameter  $\lambda$  is fitted by means of the pseudo-likelihood method, see [8], where we plug in the values  $\hat{F}(p)$  and  $\hat{G}(t)$  of the empirical distribution functions of  $F(p)$  and  $G(t)$  for  $u$  and  $v$ , respectively. This means that we divide the problem of estimating the parameters of the bivariate distribution function of  $P$  and  $\tau^{(r)}$  into two parts. First, in Section 3.1, the parameters of the univariate distribution functions are fitted. Then, in the present section, we only compute the estimate  $\hat{\lambda}$  for the parameter  $\lambda$  of the Gumbel copula, which models the dependence between local porosity and local values of  $\tau^{(0)}$ ,  $\tau^{(1.5)}$ , and  $\tau^{(3.0)}$ , respectively. The values of  $\hat{\lambda}$  are summarized in Table 1. This method of parameter estimation has the advantage that the computation of  $\hat{\lambda}$  does not depend on the parametric models used for the univariate marginal distributions. Thereby, it is guaranteed that the estimated values  $\hat{\lambda}$  reflect only the interdependence between local porosity and the local path length related descriptors.

### 3.3 Validation of the copula model

A goodness of fit test is performed to validate the choice of Gumbel copulas for modeling the joint distribution of local porosity and the mean length of local shortest transportation paths. For this purpose, we use a goodness of fit test proposed in [9]. This test compares the fitted parametric copulas model to the so-called

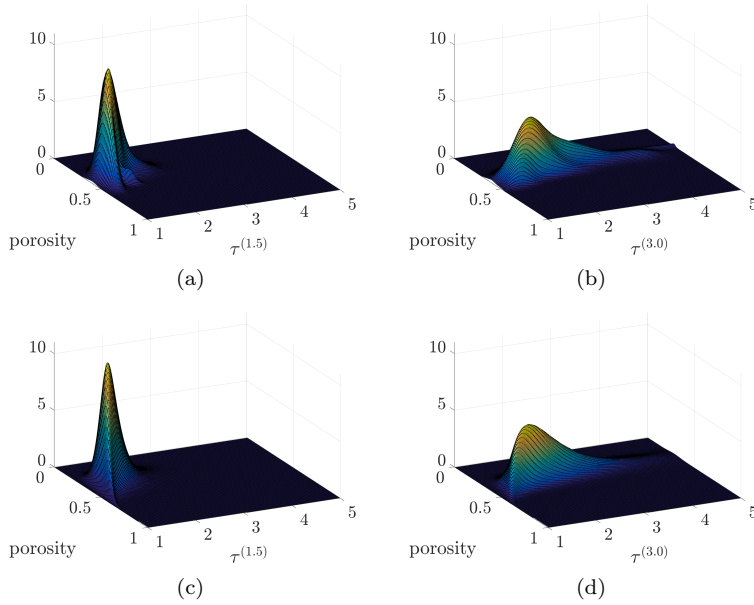


**Fig. 4** Comparison between two bivariate probability density distributions computed empirically from image data (a,b) and from the corresponding fitted parametric model, respectively (c,d). The bivariate distributions are shown for  $\tau^{(1.5)}$  with a cutout side length of  $60 \mu\text{m}$  (a,c) and for  $\tau^{(3.0)}$  with a cutout side length of  $90 \mu\text{m}$  (b,d).

empirical copula  $\hat{C}_N$ , *i.e.*, a bivariate distribution function that is computed non-parametrically from observed data.

For a number of observations  $N$ , we consider the pairs of local porosity and the corresponding value of  $\tau^{(0)}$ ,  $\tau^{(1.5)}$  or  $\tau^{(3.0)}$  denoted by  $(P_1, \tau_1^{(r)}), \dots, (P_N, \tau_N^{(r)})$ . Similar to the estimation of the copula parameter  $\lambda$ , we consider the sequence of random vectors  $(U_1, V_1), \dots, (U_N, V_N)$  defined via  $U_i = \hat{F}(P_i)$  and  $V_i = \hat{G}(\tau_i^{(r)})$  for each  $i = 1, \dots, N$ . Then, the empirical copula  $\hat{C}_N : [0, 1]^2 \rightarrow [0, 1]$  is given by

$$\hat{C}_N(u, v) = \frac{1}{N} \sum_{i=1}^N \mathbb{1}_{U_i \leq u} \mathbb{1}_{V_i \leq v} \quad (7)$$

for all  $0 \leq u, v \leq 1$ . To evaluate the discrepancy between the empirical copula and the fitted copula model, we consider the Cramér-von-Mises-type test statistic

$$S_N = \sum_{i=1}^N (\hat{C}_N(U_i, V_i) - C_{\hat{\lambda}}(U_i, V_i))^2, \quad (8)$$

where  $C_{\hat{\lambda}}$  is the Gumbel copula fitted as described in Section 3.2. Then, by means of the statistic  $S_N$ , given in Equation (8), the hypothesis  $H_0$  that the underlying copula  $C$  of the random vector  $(P, \tau^{(r)})$  belongs to the Gumbel family is tested against the alternative  $H_1$  that  $C$  is not in the Gumbel family. The corresponding  $p$ -values are determined via Monte-Carlo simulation using the parametric bootstrap (with 10000 replications) implemented in the statistical software package

**Table 2** The  $p$ -values corresponding to the goodness of fit test for different cutout sizes and tortuosities  $\tau^{(0)}$ ,  $\tau^{(1.5)}$  and  $\tau^{(3.0)}$ .

side length of cutouts	30 $\mu\text{m}$	60 $\mu\text{m}$	90 $\mu\text{m}$	120 $\mu\text{m}$	150 $\mu\text{m}$
$p$ -value for $\tau^{(0)}$	0.20	0.22	0.23	0.38	0.42
$p$ -value for $\tau^{(1.5)}$	0.45	0.10	0.41	0.75	0.35
$p$ -value for $\tau^{(3.0)}$	0.49	0.08	0.77	0.61	0.43

**Table 3** Mean values and empirical standard deviations of porosity,  $\tau^{(0)}$ ,  $\tau^{(1.5)}$  and  $\tau^{(3.0)}$  for different cutout sizes.

side length of cutouts	30 $\mu\text{m}$	60 $\mu\text{m}$	90 $\mu\text{m}$	120 $\mu\text{m}$	150 $\mu\text{m}$
porosity	$0.35 \pm 0.11$	$0.35 \pm 0.08$	$0.35 \pm 0.06$	$0.35 \pm 0.06$	$0.35 \pm 0.05$
$\tau^{(0)}$	$1.46 \pm 0.25$	$1.45 \pm 0.20$	$1.44 \pm 0.17$	$1.43 \pm 0.15$	$1.43 \pm 0.13$
$\tau^{(1.5)}$	$1.56 \pm 0.31$	$1.54 \pm 0.26$	$1.53 \pm 0.21$	$1.52 \pm 0.19$	$1.52 \pm 0.16$
$\tau^{(3.0)}$	$2.36 \pm 0.99$	$2.32 \pm 0.92$	$2.29 \pm 0.85$	$2.29 \pm 0.78$	$2.29 \pm 0.72$

R [23] as described in [15]. The obtained  $p$ -values are shown in Table 2. For each version of tortuosity and for each cutout size, the hypothesis  $H_0$  is not rejected at the significance level of 5 %, since the minimum  $p$ -value is 0.08 ( $\tau^{(3.0)}$ , cutout size 60  $\mu\text{m}$ ). Thus we consider the Gumbel copula as an appropriate copula model for the joint distribution of local porosity and local tortuosity.

In order to illustrate the goodness of fit, two bivariate probability density functions of the parametric model are compared to those estimated from image data, see Figure 4. The bivariate probability density functions of  $(P, \tau^{(r)})$  are presented for  $r = 1.5 \mu\text{m}$  with a cutout side length of 60  $\mu\text{m}$  and for  $r = 3.0 \mu\text{m}$  with a cutout side length of 90  $\mu\text{m}$ . These cases are chosen as they are the ones with lowest and highest  $p$ -values in the goodness of fit test, respectively. A good accordance between the parametric models and the empirical distributions obtained from image data can be observed in Figure 4.

#### 4 Trends in local heterogeneity

With an appropriate parametric model for the joint bivariate distribution of local porosity and the mean length of local shortest transportation paths at hand (*cf.* Section 3), we now inspect more closely the trends obtained for the local porosity,  $\tau^{(0)}$ ,  $\tau^{(1.5)}$ ,  $\tau^{(3.0)}$ , and their interdependence.

Figure 3 shows the univariate empirical distributions of the considered morphological characteristics computed from image data and the corresponding estimated distributions of the parametric model. For local porosity,  $\tau^{(0)}$ ,  $\tau^{(1.5)}$  and  $\tau^{(3.0)}$ , we can observe a decreasing variance with increasing cutout sizes, while the mean values approximately remain the same, see Table 3.

In terms of the minimal path diameter  $r$ , we find the relation  $\tau^{(r_1)} \leq \tau^{(r_2)}$  confirmed for all  $r_1 \leq r_2$  and all cutouts, since each path, that permits a ball with a radius  $r_2$  to pass, readily admits a ball of a smaller radius  $r_1$ . Moreover, note that an increase of  $r$  not only causes a monotonous increase in the mean value  $\tau^{(r)}$

(*cf.* Figure 3e-f), see [16], but also in the variances of  $\tau^{(r)}$  (*cf.* Table 3). The latter trend is caused by the fact that the number of those shortest transportation paths, that are significantly longer than the corresponding mean value, increases with increasing  $r$ . The increasing contribution of longer pathways becomes particular apparent when comparing  $\tau^{(1.5)}$  with  $\tau^{(3.0)}$  (Figure 3e-f).

The local porosity and the local lengths of transportation paths are negatively correlated for all cutout sizes, independent whether  $\tau^{(0)}$ ,  $\tau^{(1.5)}$ , or  $\tau^{(3.0)}$  is concerned. A negative correlation between porosity and tortuosity can be readily expected, as a lower porosity should hamper the formation of shorter pathways. This relationship has been theoretically demonstrated for simple geometrical microstructure models [10]. In our case, the negative correlation is an inherent consequence of the fact that the Gumbel copula is appropriate to model the joint distribution of local porosity and local tortuosity (validated in Section 3.3)<sup>1</sup>. The parameter  $\lambda$  of the Gumbel copula quantifies the correlation between local porosity and local tortuosity, *i.e.*, the larger  $\lambda$  is the stronger is the negative correlation.

The estimators  $\hat{\lambda}$  for  $\lambda$ , collected in Table 1, reveal in particular: (i)  $\hat{\lambda}$  increases with the cutout size for each  $\tau^{(0)}$ ,  $\tau^{(1.5)}$ , and  $\tau^{(3.0)}$ ; (ii)  $\hat{\lambda}$  indicates that porosity correlates most strongly with  $\tau^{(1.5)}$  followed by  $\tau^{(0)}$  and  $\tau^{(3.0)}$ ; and (iii) for the largest cutout size of 150  $\mu\text{m}$ , the values of  $\hat{\lambda}$  for  $\tau^{(0)}$ ,  $\tau^{(1.5)}$ , and  $\tau^{(3.0)}$  are close to each other.

The dependence of  $\hat{\lambda}$  on the cutout size, stated in (i), is readily rationalized by considering the computation of the mean geodesic tortuosity. In the latter, we consider all those paths, whose starting points are located in the corresponding cutout, while the path itself is allowed to leave the cutout. The more paths start in a cutout that the paths eventually leave, the less is the correlation with the porosity of this cutout. The length of those paths depends also on the local porosity in the neighborhood of the considered cutout. Since the amount of paths leaving the cutout is larger for smaller cutouts, it is reasonable that  $\hat{\lambda}$  increases with the cutout size. Under mild conditions, *e.g.*, in case that the shortest path lengths are bounded from above by some constant<sup>2</sup>, the impact of paths leaving the cutout vanishes when the cutout size tends to infinity [20]. Under these conditions we would assume that  $\hat{\lambda}$  converges to a constant value if the cutout size tends to infinity.

To rationalize (ii), *i.e.*, why  $\tau^{(1.5)}$  appears to correlate most strongly, two competing effects have to be taken into account. On the one hand,  $\tau^{(r)}$  of a cutout considers those transportation pathways, that possess a minimal diameter of at least  $r$  and that originate in the cutout. The larger  $r$ , the more of these transportation pathways tend to leave the cutout, because the paths become longer in general. In combination with the argument put forward in (i), increasing  $r$  translate into decreasing values of  $\hat{\lambda}$ . On the other hand, the larger  $r$ , the more pores are necessary to form short transportation paths that permit the passage of balls

<sup>1</sup> Recall from Section 3.2 that we use the Gumbel copula to model the joint distribution of the random vector  $(P, -\tau^{(r)})$ , where  $P$  and  $\tau^{(r)}$  denote the porosity and the random value of mean geodesic tortuosity or one of its modifications, respectively, in a cutout of predefined size. Since the Gumbel copula allows only to model the joint distribution of positively correlated random variables, the random variables  $P$  and  $\tau^{(r)}$  are negatively correlated.

<sup>2</sup> More precisely, we mean that the shortest path length of each starting point at the bottom surface is bounded by some constant, provided that there exists a path from this starting point to the top surface.

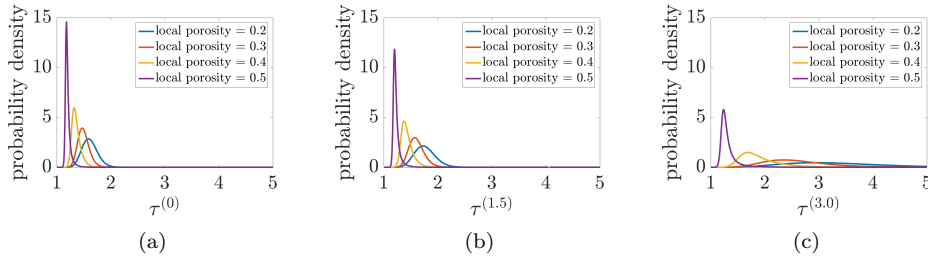


**Fig. 5** Conditional distributions of  $\tau^{(0)}$  (a),  $\tau^{(1.5)}$  (b) and  $\tau^{(3.0)}$  (c) for given local porosities computed by means of the copula model. The cutout size is 150  $\mu\text{m}$ .

of radius  $r$ . This effect leads to increasing values of  $\hat{\lambda}$  for increasing  $r$ . In going from  $\tau^{(0)}$  with  $\tau^{(1.5)}$  (*cf.* Table 1), the latter effect is stronger. However, when going further to  $\tau^{(3.0)}$ , the former effect appears to dominate.

The competition between the two aforementioned effects also rationalizes observation (iii), *i.e.*, that large cutout sizes yield rather similar values of  $\hat{\lambda}$  for  $\tau^{(0)}$ ,  $\tau^{(1.5)}$  and  $\tau^{(3.0)}$ . It is remarkable that the interdependence between porosity and  $\tau^{(0)}$ ,  $\tau^{(1.5)}$  and  $\tau^{(3.0)}$  is predicted to be similar for a cutout size of 150  $\mu\text{m}$ , even though the marginal distributions of  $\tau^{(0)}$ ,  $\tau^{(1.5)}$  and  $\tau^{(3.0)}$  are markedly different (*cf.* red curves in Figure 2). Apparently, the two competing effects that dictate the relationship between  $r$  and  $\hat{\lambda}$  are balanced most equally for the particular cutout size of 150  $\mu\text{m}$ . Since the effect of transportation paths leaving the cutout is assumed to vanish for increasing cutout sizes, we conjecture that  $\hat{\lambda}$  remains dependent on  $r$ , in fact, keeps monotonously increasing, for cutouts of even larger size. To underpin this conjecture, further investigations with respect to the relationship between local porosity and local values of  $\tau^{(r)}$  would be necessary, where more values of  $r$  and larger cutout sizes have to be taken into account.

Besides the quantification of the interdependence between local tortuosity and local porosity, we obtain the conditional distributions of  $\tau^{(0)}$ ,  $\tau^{(1.5)}$  and  $\tau^{(3.0)}$  for a given local porosity directly from Equation (5). Examples of such conditional distributions derived from the copula model are shown in Figure 5 for a cutout size of 150  $\mu\text{m}$ . Here one can observe that the skewness of the conditional distributions decreases with increasing local porosity. Once having established such conditional distributions, they can be used to predict intervals, in which the values of  $\tau^{(0)}$ ,  $\tau^{(1.5)}$  and  $\tau^{(3.0)}$  are located with a certain probability for a given local porosity. This is particularly appealing, since porosity can be – contrary to  $\tau^{(0)}$ ,  $\tau^{(1.5)}$  and  $\tau^{(3.0)}$  – experimentally determined. Thus, based on the knowledge of porosity, the presented methodology helps to predict the behavior of further morphological characteristics, which are meaningful for the air permeance in sack paper.

## 5 Conclusions

In the present article, we have parametrically modeled the joint distribution of local porosity and local morphological characteristics describing the lengths of shortest transportation paths in sack paper, which has been recently investigated with respect to global characteristics in [16]. For this purpose, we have considered

cutouts of 3D image data obtained by  $\mu$ -CT and studied the variability and interdependence of the considered morphological characteristics for different sizes of cutouts. We proposed a copula model which allows for a quantification of the joint distribution by means of its model parameter. The obtained results show how the interdependence between local porosity and local values of  $\tau^{(r)}$ , *i.e.*, of tortuosity, where only paths with a certain minimum diameter are considered, changes with  $r \geq 0$ . Briefly summarizing the results of Section 4, local porosity and local values of  $\tau^{(0)}$ ,  $\tau^{(1.5)}$  and  $\tau^{(3.0)}$  are negatively correlated, the interdependence becomes stronger with increasing cutout size and no monotonicity (in  $r$ ) of the interdependence is observed. Moreover, by the aid of the model, we compute the conditional distribution of  $\tau^{(0)}$ ,  $\tau^{(1.5)}$  and  $\tau^{(3.0)}$  given the local porosity of a cutout. Doing so, we give deeper insights regarding the influence of local porosity on the windedness of shortest transportation paths through the pore space of sack paper, which is important to better understand the impact of local porosity on local air permeance - a key property of sack paper.

## Appendix

In addition to Section 3.1, we provide the numerical values of the fitted parameters regarding the univariate distributions of porosity,  $\tau^{(0)}$ ,  $\tau^{(1.5)}$ , and  $\tau^{(3)}$  in Tables 4, 5, 6, and 7, respectively. Moreover, the corresponding  $p$ -values of the Kolmogorov-Smirnov test indicating the goodness of fit are shown. Since our sample consists of 204 observations, the  $p$ -values are simulated based on the procedure proposed in [17], rather than using the ones of the asymptotic case. For this purpose, we make use of the implementation in the statistical software package R [23].

**Table 4** Estimated values  $\hat{a}$  and  $\hat{b}$  for the parameters  $a$  and  $b$  of the beta-distribution modeling the univariate distribution of porosity. Moreover, the  $p$ -values corresponding to the Kolmogorov-Smirnov test for different cutout sizes are shown.

side length of cutouts	30 $\mu\text{m}$	60 $\mu\text{m}$	90 $\mu\text{m}$	120 $\mu\text{m}$	150 $\mu\text{m}$
$\hat{a}$	6.15	12.53	19.54	25.19	29.38
$\hat{b}$	11.49	23.63	36.39	46.82	54.69
$p$ -value	0.90	0.99	0.99	0.95	0.72

**Table 5** Estimated values  $\hat{\alpha}$ ,  $\hat{d}$ , and  $\hat{k}$  for the parameters  $\alpha$ ,  $d$  and  $k$  of the shifted generalized gamma distribution modeling the univariate distribution of  $\tau^{(0)}$ . Moreover, the  $p$ -values corresponding to the Kolmogorov-Smirnov test for different cutout sizes are shown.

side length of cutouts	30 $\mu\text{m}$	60 $\mu\text{m}$	90 $\mu\text{m}$	120 $\mu\text{m}$	150 $\mu\text{m}$
$\hat{\alpha}$	0.137	0.017	0.013	0.016	0.014
$\hat{d}$	1.02	0.72	0.75	0.81	0.85
$\hat{k}$	3.49	7.37	9.98	11.85	15.15
$p$ -value	0.54	0.88	0.85	0.88	0.80

**Table 6** Estimated values  $\hat{\alpha}$ ,  $\hat{d}$ , and  $\hat{k}$  for the parameters  $\alpha$ ,  $d$  and  $k$  of the shifted generalized gamma distribution modeling the univariate distribution of  $\tau^{(1.5)}$ . Moreover, the  $p$ -values corresponding to the Kolmogorov-Smirnov test for different cutout sizes are shown.

side length of cutouts	30 $\mu\text{m}$	60 $\mu\text{m}$	90 $\mu\text{m}$	120 $\mu\text{m}$	150 $\mu\text{m}$
$\hat{\alpha}$	0.188	0.033	0.025	0.011	0.020
$\hat{d}$	1.02	0.75	0.78	0.72	0.84
$\hat{k}$	3.12	5.95	8.24	11.81	12.96
$p$ -value	0.88	0.95	0.80	0.92	0.92

**Table 7** Estimated values  $\hat{\alpha}$ ,  $\hat{d}$ , and  $\hat{k}$  for the parameters  $\alpha$ ,  $d$  and  $k$  of the shifted generalized gamma distribution modeling the univariate distribution of  $\tau^{(3.0)}$ . Moreover, the  $p$ -values corresponding to the Kolmogorov-Smirnov test for different cutout sizes are shown.

side length of cutouts	30 $\mu\text{m}$	60 $\mu\text{m}$	90 $\mu\text{m}$	120 $\mu\text{m}$	150 $\mu\text{m}$
$\hat{\alpha}$	0.066	0.017	0.005	0.009	0.013
$\hat{d}$	0.59	0.51	0.47	0.52	0.56
$\hat{k}$	3.32	4.47	5.92	6.53	7.15
$p$ -value	0.97	0.86	0.93	0.30	0.30

## References

- Alajami, A., Li, Y., Kloppenburg, G., Simon, J.W.: Evaluating the mechanical response of fiber networks with RVEs. In: Proceedings of the International Paper Physics Conference, pp. 51–56. TAPPI, Indianapolis (2019)
- Axelsson, M., Svensson, S.: 3D pore structure characterisation of paper. *Pattern Analysis and Applications* **13**(2), 159–172 (2010)
- Beckman, R.J., Tietjen, G.L.: Maximum likelihood estimation for the beta distribution. *Journal of Statistical Computation and Simulation* **7**(3-4), 253–258 (1978)
- Beneš, V., Stepán, J.: *Distributions with given Marginals and Moment Problems*. Springer, Dordrecht (2012)
- Chinga, G., Helle, T.: Structure characterisation of pigment coating layer on paper by scanning electron microscopy and image analysis. *Nordic Pulp and Paper Research Journal* **17**(3), 307–312 (2002)
- Chiu, S.N., Stoyan, D., Kendall, W.S., Mecke, J.: *Stochastic Geometry and its Applications*, 3rd edn. J. Wiley & Sons, Chichester (2013)
- Dirrenberger, J., Forest, S., Jeulin, D.: Towards gigantic RVE sizes for 3D stochastic fibrous networks. *International Journal of Solids and Structures* **51**(2), 359–376 (2014)
- Genest, C., Ghouli, K., Rivest, L.P.: A semiparametric estimation procedure of dependence parameters in multivariate families of distributions. *Biometrika* **82**(3), 543–552 (1995)
- Genest, C., Rémillard, B., Beaudoin, D.: Goodness-of-fit tests for copulas: A review and a power study. *Insurance: Mathematics and Economics* **44**(2), 199–213 (2009)
- Ghanbarian, B., Hunt, A.G., Ewing, R.P., Sahimi, M.: Tortuosity in porous media: a critical review. *Soil Science Society of America Journal* **77**(5), 1461–1477 (2013)
- Gurnagul, N., Shallhorn, P., Omholt, I., Miles, K.: Pressurised high-consistency refining of kraft pulps for improved sack paper properties. *Appita Journal: Journal of the Technical Association of the Australian and New Zealand Pulp and Paper Industry* **62**(1), 25 (2009)

12. Hassan, A.E., Cushman, J.H., Delleur, J.W.: Significance of porosity variability to transport in heterogeneous porous media. *Water Resources Research* **34**(9), 2249–2259 (1998)
13. Johnson, N.L., Kotz, S., Balakrishnan, N.: *Continuous Univariate Distributions*. J. Wiley & Sons, New York (1995)
14. Kanit, T., Forest, S., Galliet, I., Mounoury, V., Jeulin, D.: Determination of the size of the representative volume element for random composites: statistical and numerical approach. *International Journal of Solids and Structures* **40**, 3647–3679 (2003)
15. Kojadinovic, I., Yan, J.: Modeling multivariate distributions with continuous margins using the copula R package. *Journal of Statistical Software* **34**(9), 1–20 (2010)
16. Machado Charry, E., Neumann, M., Lahti, J., Schennach, R., Schmidt, V., Zojer, K.: Pore space extraction and characterization of sack paper using  $\mu$ -CT. *Journal of Microscopy* **272**(1), 35–46 (2018)
17. Marsaglia, G., Tsang, W.W., Wang, J.: Evaluating Kolmogorov’s distribution. *Journal of Statistical Software* **8**(18), 1–4 (2003)
18. Nelder, J.A., Mead, R.: A simplex method for function minimization. *The Computer Journal* **7**, 308–313 (1965)
19. Nelsen, R.B.: *An Introduction to Copulas*. Springer, New York (2007)
20. Neumann, M., Hirsch, C., Staněk, J., Beneš, V., Schmidt, V.: Estimation of geodesic tortuosity and constrictivity in stationary random closed sets. *Scandinavian Journal of Statistics* **46**, 848–884 (2019)
21. Neumann, M., Machado Charry, E., Leitl, P., Hirn, U., Zojer, K., Schmidt, V.: Joint distribution of local porosity and local tortuosity in sack paper. In: *Proceedings of the International Paper Physics Conference*, pp. 100–105. TAPPI, Indianapolis (2019)
22. Ohser, J., Schladitz, K.: *3D Images of Materials Structures: Processing and Analysis*. J. Wiley & Sons, Weinheim (2009)
23. R Core Team: *R: A Language and Environment for Statistical Computing*. R Foundation for Statistical Computing, Vienna, Austria (2015)
24. Rolland du Roscoat, S., Decain, M., Thibault, X., Geindreau, C., Bloch, J.F.: Estimation of microstructural properties from synchrotron X-ray microtomography and determination of the REV in paper materials. *Acta Materialia* **55**(8), 2841–2850 (2007)
25. Schweizer, B.: Thirty years of copulas. In: G. Dall’Aglia, S. Kotz, G. Salinetti (eds.) *Advances in Probability Distributions with given Marginals*, pp. 13–51. Kluwer Academic Publishers, Dordrecht (1991)
26. Serra, J.: *Image Analysis and Mathematical Morphology*. Academic Press, London (1982)
27. Thovert, J.F., Yousefian, F., Spanne, P., Jacquin, C.G., Adler, P.M.: Grain reconstruction of porous media: application to a low-porosity Fontainebleau sandstone. *Physical Review E* **63**(6), 061307 (2001)
28. Thulasiraman, K., Swamy, M.N.S.: *Graphs: Theory and Algorithms*. J. Wiley & Sons, New York (1992)
29. Torquato, S.: *Random Heterogeneous Materials: Microstructure and Macroscopic Properties*. Springer, New York (2002)